Original scientific paper

DUAL BAND MIMO ANTENNA FOR LTE, 4G AND SUB–6 GHZ 5G APPLICATIONS

Pinku Ranjan[1], Swati Yadav[2], Amit Bage[3]

[1]Department of Electrical / Electronic Engineering, Atal Bihari Vajpayee-Indian Institute of Information Technology and Management (ABV-IIITM), Gwalior, India
[2]Department of Electronics & Telecommunication Engineering, College of Engineering Roorkee, Uttarakhand-247667, India
[3]Department of Electronics and Communication Engineering, National Institute of Technology, Hamirpur, India

Abstract. *In this manuscript, a compact MIMO antenna for wireless application has been presented. The proposed antenna consists of the F-shaped radiator with the circular slot in the center and a rectangular ground plane on the other side of the substrate. The proposed antenna has the overall size of 48 × 48 mm2. The antenna is designed to work on two frequency bands - from 1.5 to 2.3 GHz, and 3.7 to 4.2 GHz, having the resonating frequency of 1.8 GHz and 3.9 GHz respectively. The diversity performance of the antenna is also observed by using a variety of parameters like envelop correlation coefficient (ECC), Diversity Gain (DG), Total Active Reflection Coefficient (TARC), etc. The value of ECC is 0.02, which shows good diversity performance of the antenna. In order to validate the simulated and measured results, the proposed antenna has been fabricated and shows good agreement with the each other.*

Key words: *MIMO antenna; Envelop correlation coefficient (ECC); Total Active Reflection Coefficient (TARC)*

1. 1. INTRODUCTION

In worldwide terms, wireless communication is considered to be the fastest growing technology. In 2020, it is expected that 70 percent of the world's population will have at least a smart phone. The improvement in the generation of wireless communication in terms of data rate, antenna size and higher gain are required. A technology that fulfills the higher demands of such future wireless communication is the use of multiple input multiple output (MIMO) antennas.

In MIMO antenna design technology, multiple antennas are used on both transmitting and receiving side in order to increase the radio link capacity. In this technique, more than

one data signal is simultaneously transmitted or received over the same radio channel. By using the MIMO technology, the signal capturing capacity of receiver is increased by allowing antennas to combine their data streams that are arriving from different paths at different times. MIMO is the most important technique in most of the research and will play a key role in the next generation wireless systems, including 5G networks. For the MIMO antenna system, isolation between the two radiating elements is very important. Therefore, two radiators should be designed in such a way that the isolation between them is less than –15 dB. To ensure the isolation between the antenna elements with a miniaturized size is a big challenge for the antenna designers. In the past few years many researches have proposed different MIMO antennas with different techniques [1]–[10]. In [11], antenna with two-element semi-ring along with UWB amplifier is presented to design MIMO antenna. An annular slot antenna and two shorts in the opposite direction placed at 45 degrees between the microstrip lines are used to achieve an isolation [12]. In 2018 [13], A. Dkiouak et al. presented a compact MIMO antenna for wireless application based on two symmetrical monopoles with a T-shape junction. The T-shape junction is used to enhance the isolation between two antennas. To abandon the reactive coupling connection between the different antenna elements of MIMO antenna, the technique of parasitic elements is used [14]. In [15], a high isolated compact 2 x 2 MIMO antenna is designed using PIFA and DGS has been used to improve the inter port isolation.

In this proposed design, a simple F–shaped radiator is used to get the dual band function of the MIMO antenna for the wireless communication. The F–shaped radiator is chosen to get the desired band of application. The antenna has been designed to work at two different frequency bands ranging from 1.5 - 2.3 GHz and 3.7 - 4.2 GHz, and having the resonating frequency of 1.8 GHz and 3.9 GHz respectively. The numerical analysis has been carried out using High Frequency Simulation Software (HFSS). The organization of the manuscript is as follows. In section 2, antenna design and configuration are presented with its design steps. In section 3, simulated and measured return loss, isolation between ports and radiation pattern are presented. In section 4, diversity performance is evaluated in terms of ECC, TARC, and DG. Finally, conclusion is provided in section 5.

2. ANTENNA DESIGN AND CONFIGURATION

2.1. Methodology

The flowchart of the proposed antenna from design specification to fabrication and measurement is shown in Fig. 1. The design methodology of the proposed MIMO antenna starts from the antenna design specification. After the design specification a single element antenna is designed with the desired frequency response. The single element antenna is modified to a double element square patch MIMO antenna. In order to achieve the desired MIMO characteristics and frequency ranges, F-shaped MIMO antenna is designed with a circular slot. In the next step, the optimization of all the parameters of the designed antennas is done to check its performance. Once the desired performance is achieved, the proposed antenna is fabricated and measured.
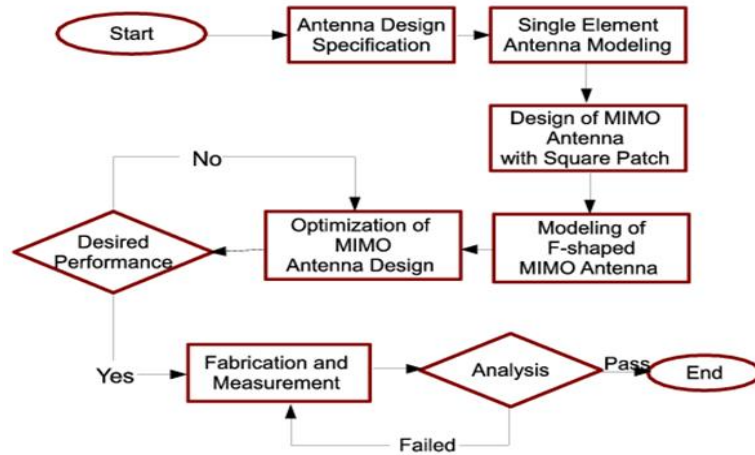
Fig. 1 Flow diagram represents antenna specification to fabrication

2.2. Design Parameter

The front view and back view of the proposed antenna with its dimensions are shown in Fig. 2. The antenna has been designed on FR-4 dielectric substrate having thickness = 1.6 mm, copper thickness = 0.035 mm, dielectric constant = 4.4, and loss tangent = 0.02. The overall dimensions of the proposed antenna are 48×48 mm^2. The antenna consists of two radiating elements of F-shape, which are placed horizontally to each other on top side of substrate along with the rectangular ground plane, which is designed on the bottom side of the dielectric substrate. The design steps of the proposed antenna are shown in Fig. 3. In order to achieve the desired characteristics, there are three design steps. At first, a square

(a)   (b)
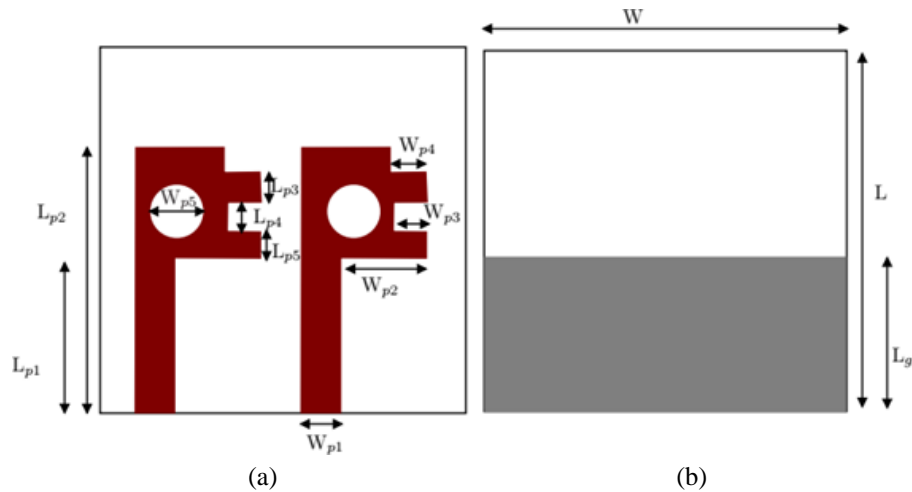
Fig. 2 (a) Top view and (b) bottom view of proposed antenna where L = 48, Lp1= 23, Lp2= 41, Lp3= 4, Lp4= 6, Lp5= 5, W= 48, Wp1=3, Wp2 = 13, Wp3 = 4, Wp4 = 5, Wp5 = 8 and Lg1 =20 (all in mm)

shape radiator is designed along with the microstrip feed line as shown in Fig. 3(a). The square shape antenna shows the dual band performance with 1.4 – 2.3 GHz and 3.9 – 4.4 GHz bands, which is not the desired operating frequency bands. Also, for the square shaped antenna, the second operating band shows low impedance matching.
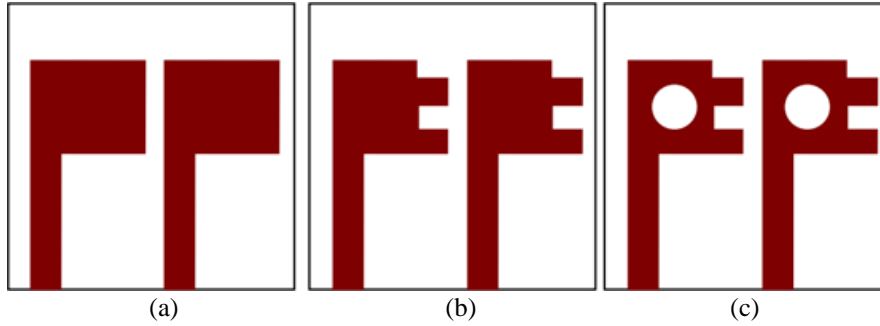
Fig. 3 Evolution of the Proposed Antenna (a) Antenna 1 (b) Antenna 2 (c) Antenna 3

As a result, two F-shape slots are etched from the radiator in the next stage as shown in Fig. 2(b). The two F-slots etched from rectangular patch with different dimensions. This F–shaped antenna operates in the 1.5–2.3 GHz and 3.8–4.3 GHz frequency ranges, which is not the required LTE and Sub-6 5G band. In order to achieve the desired frequency band, the second operating band has been shifted to the lower frequency. In order to shift at lower frequency bands, a circular slot is etched from the upper part of the rectangular patch along with F-slot. Using this circular slot the proposed antenna achieved the desired dual band performance with two operating bands from 1.8–2.3 GHz and 3.7–4.2 GHz. The width of the microstrip feed is kept same for all the three design and is equal to 3 mm. The gap between the two radiators is 8 mm. The simulated S-parameters for the Fig. 3 is shown in Fig. 4. The Fig. 4(a) reveals that antenna 3 which is the F–shaped structure with circular slot shows good performance. It is also clear from the Fig. 4(b), the designed F–shaped antenna shows the good impedance matching over the two frequency bands with the center
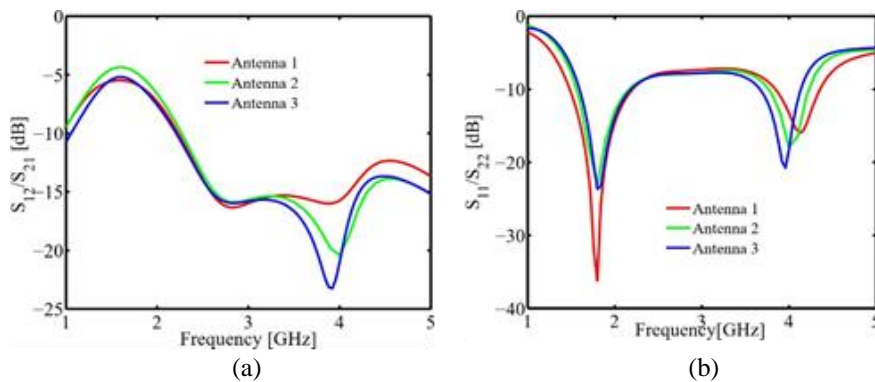
Fig. 4 (a) Simulated S_{12}/S_{21} parameter versus frequency for antenna 1, 2 and 3 and (b) simulated S_{11}/S_{22} parameters versus frequency for antenna 1, 2 and 3

frequency of 1.8 GHz and 3.9 GHz, and the isolation between the two antennas is less than –5, and –15 dB for the two bands. To analyze the behavior of antenna current densities for the two different frequencies are determined. For calculating the current densities at two resonating frequencies Port 1 is excited.

The current distribution of the proposed antenna at 1.8 and 3.9 is shown in Fig. 5.

(a)   (b)
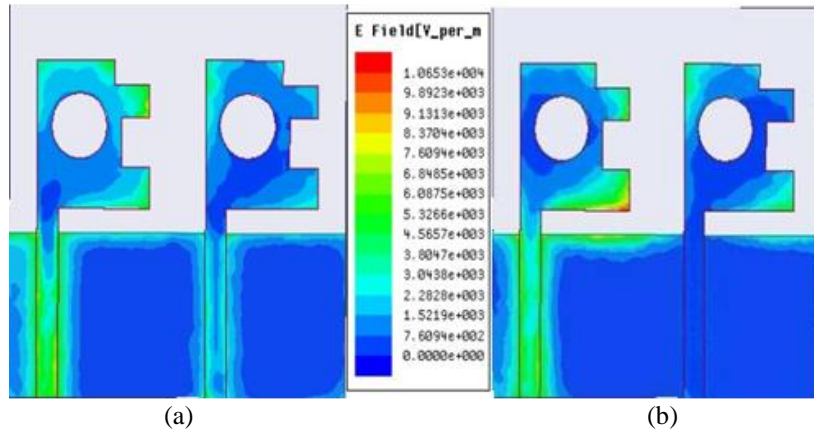
Fig. 5 Surface current densities at (a) 1.8 GHz and (b) 3.9 GHz

The figure reveals that, at 1.8 GHz resonant frequency the surface current is uniformly distributed at the feed line and the lower part of the F-shaped radiator. For the frequency of 3.9 GHz the current is uniformly distributed at the lower strip of the F-shaped structure.

3. RESULT AND DISCUSSION

In order to validate the numerical analysis, the proposed dual band MIMO antenna has been fabricated using PCB prototype machine. The fabricated top view and bottom view are shown in Fig. 6. The fabricated antenna is measured using Agilent N5230A vector network analyzer.

(a)   (b)
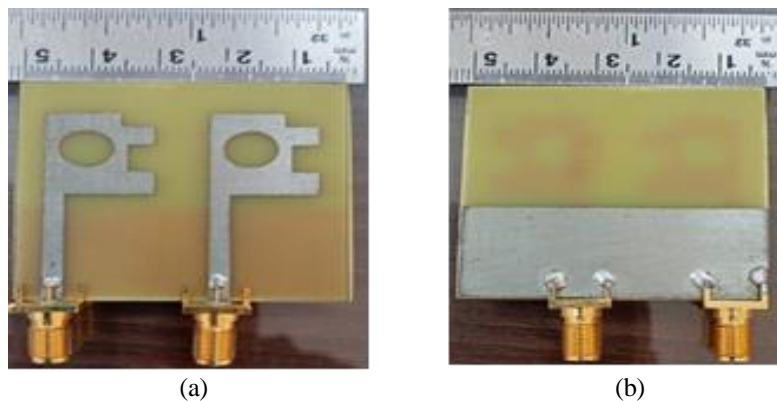
Fig. 6 Fabricated photograph of the proposed dual band MIMO antenna, (a) top view, and (b) bottom view

    The simulated and measured S-parameters (S11/S22 and S12/S21) are compared and shown in Fig. 7. The figure shows that they are in good agreement with each other. The measurement of radiation patterns is performed inside an anechoic chamber for each element, by keeping the other element terminated with matched load. The radiation pattern at two different frequencies is calculated for the two principal planes (E-plane and H- plane) as shown in Fig. 8.

(a)   (b)
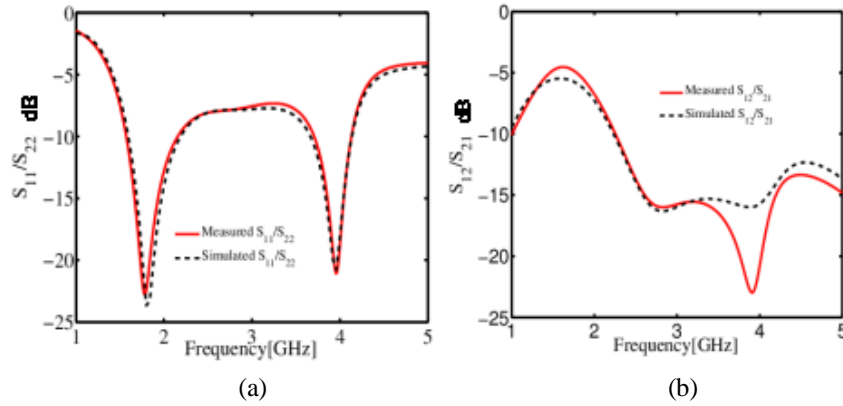
Fig. 7 The comparison of simulated and measured results (a) S_{11}/S_{22} dB and (b) S_{12}/S_{21} dB

(a)

(b)
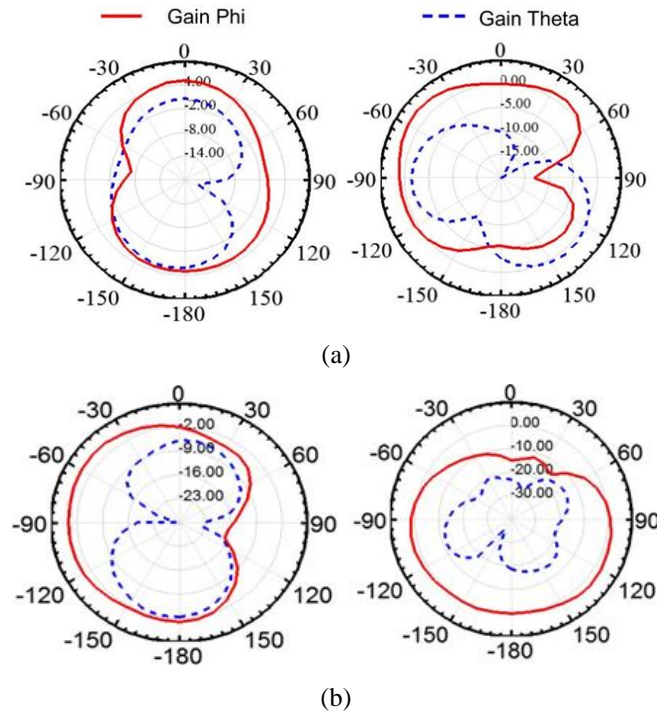
Fig. 8 Simulated Radiation Pattern for Proposed Antenna at (a) at 1.8 GHz and (b) 3.9 GHz

The Fig. 8(a) shows the simulated radiation pattern of the proposed antenna at 1.8 GHZ for E and H plane, and the radiation pattern at the 3.9 GHz for E and H plane frequency is shown in the Fig. 8(b). The figure evidences that the antenna possesses the consistent radiation pattern for both frequency bands. Fig. 9 shows the gain of the presented antenna for the two different frequency bands. From the figure, it is clear the designed antenna possesses the gain of around 4 dB and 2 dB for the 1.8 GHz and 3.9 GHz frequency respectively.
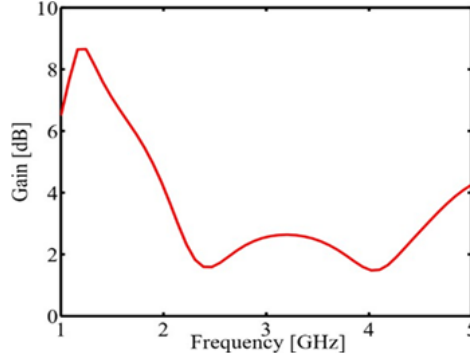
Fig. 9 Simulated gain verses frequency graph for the proposed dual band MIMO antenna

A comparison of the characteristics of proposed MIMO antenna with few other reported MIMO antenna [11, 12, 13, 14 and 15] is tabulated in Table 1.

Table 1 Comparison of presented antenna with previous literature

Ref.	Impedance BW (GHz)	Isolation (dB)	Size (in mm)	Electrical Size in guided wavelength	ECC
[11]	1.8–5.5	-12	50×90×0.76	1.13× 2.0486 × 0.0173	0.33
[12]	3–12	-15	80×80×0.6	4.19 × 4.19 × 0.031	-
[13]	2.35–3.05 and 5.12–5.51	-12	43×37×1.6	0.811× 0.69 × 0.0302	0.001
[14]	3.2–3.7, 5.1–5.6, 6.7 7.5	-30	70×50×0.6	1.6886 × 1.2061 × 0.0145	-
[15]	5.2 – 6	-25	100×50×0.8	3.95 × 1.97 × 0.0316	<0.5
Proposed Antenna	1.5 – 2.3 and 3.3 –4.2	-15	48×48×1.6	0.6377 × 0.6377 × 0.0213	<0.002

4. DIVERSITY PERFORMANCE

For MIMO antenna, the diversity performance shows how efficiently two antennas work individually. The diversity performance can be calculated using different parameters such as Envelop Correlation Coefficient (ECC), Diversity Gain (DG), Total Active Reflection Coefficient (TARC), etc. The capacity to receive information individually by each antenna is shown through ECC. To achieve better performance, the value of ECC should be less than 0.2, and it can be calculated using the method proposed in [16]:

$$ECC = |S_{11}^* S_{12} + S_{21}^* S_{22}|^2 / (1 - |S_{11}|^2 - |S_{21}|^2)(1 - |S_{21}|^2 - |S_{12}|^2) \tag{1}$$

The diversity gain (DG), can be calculated using the envelop correlation coefficient. For the proposed Dual band MIMO antenna, the diversity gain can be calculated using [16]:

$$DG = \sqrt{1 - |ECC|^2} \tag{2}$$

The simulated ECC and DG of the proposed antenna is shown in Fig. 10. The figure shows that ECC of the proposed antenna is below 0.002 at both frequency bands which ensure the good diversity performance of the presented MIMO antenna. In the same figure, the diversity gain of the proposed antenna is above 9.9 dB at the resonating frequencies. In the transmission and reception process of MIMO antenna systems, working of multiple antennas together will affect the overall operating bandwidth and efficiency. The effect of multiple antenna elements on each other is shown through total active reflection coefficient (TARC). TARC can

Fig. 10 Simulated ECC and DG of the proposed antenna

be defined as square root of the ratio of total reflected power to the total incident power and is apparent return loss of the overall MIMO antenna system. For Dual-band MIMO system, the value of TARC can be calculated using the equation given in [17]:

$$TARC = \sqrt{(S_{11} + S_{12})^2 + (S_{21} + S_{22})^2}/\sqrt{2} \tag{3}$$

The value of TARC should be <0 dB for the MIMO communication. The simulated TARC of the proposed MIMO is shown in Fig. 11. The figure reveals at both resonant frequencies the TARC is below -25 dB.
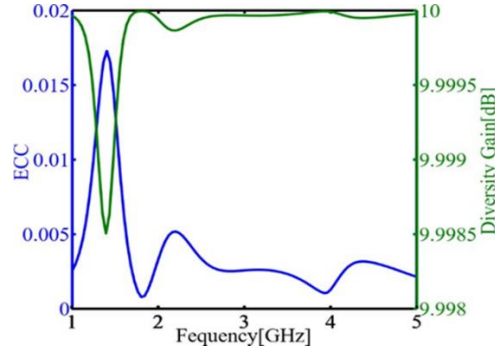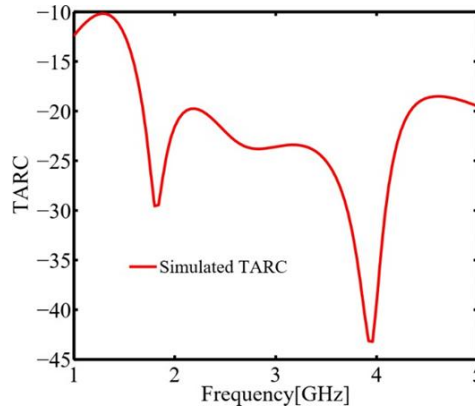
Fig. 11 Simulated TARC of the Proposed Dual Band MIMO Antenna

5. CONCLUSION

This manuscript introduces a small MIMO antenna for LTE 4G and the Sub-6 GHz 5G channel. The suggested antenna operates effectively in two frequency bands having bandwidths of 500 MHz and 600 MHz respectively and ranging from 1.8–2.3 GHz and 3.7–4.3 GHz. The measured and simulated results of the proposed antenna are compared, which shows the good agreement with each other. The antenna also shows good diversity performance with low envelop correlation coefficient, good diversity gain and low value of TARC. The radiation pattern at E–plane and H–plane for the antenna at both the resonating frequency shows the omnidirectional pattern.

REFERENCES

[1] B. X. Wang, W. Q. Huang and L. L. Wang, "Ultra-narrow terahertz perfect light absorber based on surface lattice resonance of a sandwich resonator for sensing applications", *RSC Advances*, vol. 7, pp. 42956-42963, 2017.

[2] D. Hu, T. Meng, H. Wang, Y. Ma and Q. Zhu, "Ultra-narrow-band terahertz perfect metamaterial absorber for refractive index sensing application", *Results Phys.*, vol. 19, p. 103567, 2020.

[3] F. Yan, Q. Li, H. Tian, Z. Wang and L. Li, "Ultrahigh Q-factor dual-band terahertz perfect absorber with dielectric grating slit waveguide for sensing", *J. Phys. D: Appl. Phys.*, vol. 53, p. 235103, 2020.

[4] Q. Xie, G. Dong, B. Wang and W. Huang, "Design of Quad-Band Terahertz Metamaterial Absorber Using a Perforated Rectangular Resonator for Sensing Applications", *Nanoscale Res. Lett.*, vol. 13, p. 137, 2018.

[5] M. Janneh, A. de Marcellis, E. Palange, A. T. Tenggara and D. Byun, "Design of a metasurface-based dual-band Terahertz perfect absorber with very high Q-factors for sensing applications", *Opt. Commun.*, vol. 416, pp. 152-159, 2018.

[6] W. Yin, Z. Shen, S. Li, L. Zhang and X. Chen, "A Three-Dimensional Dual-Band Terahertz Perfect Absorber as a Highly Sensitive Sensor", *Front. Phys.*, vol. 9, p. 665280, 2021.

[7] X. Hu, G. Xu, L. Wen, H. Wang, Y. Zhao, Y. Zhang, D. R. S. Cumming and Q. Chen, "Metamaterial absorber integrated microfluidic terahertz sensors", *Laser Photonics Rev.*, vol. 10, pp. 962-969, 2016.

[8] L. Cong, S. Tan, R. Yahiaoui, F. Yan, W. Zhang and R. Singh, "Experimental demonstration of ultrasensitive sensing with terahertz metamaterial absorbers: A comparison with the metasurfaces", *Appl. Phys. Lett.*, vol. 106, p. 031107, 2015.

[9] A. Kovačević, M. Potrebić and D. Tošić, "Sensitivity Analysis of Possible THz Virus Detection Using Quad-Band Metamaterial Sensor", In Proceedings of the IEEE 32nd International Conference on Microelectronics (MIEL), Niš, Serbia, 2021, pp 107-110.

[10] N. Akter, M. M. Hasan and N. Pala, "A Review of THz Technologies for Rapid Sensing and Detection of Viruses including SARS-CoV-2", *MDPI Biosensors*, vol. 11, p. 349, 2021.

[11] N. Shen, P. Tassin, T. Koschny and C. Soukoulis, "Comparison of gold- and graphene-based resonant nano-structures for terahertz metamaterials and an ultra-thin graphene-based modulator", *Phys. Rev. B,* vol. 90, no. 11, p. 115437, 2014.

[12] WIPL-D Pro 17, 3D Electromagnetic Solver, WIPL-D d.o.o., Belgrade, Serbia, 2021. Available online: http://www.wipl-d.com (accessed on 29 April 2022).

[13] B. Dadonaite, B. Gilbertson, M. L. Knight, S. Trifković, S. Rockman, A. Laederach, L. E. Brown, E. Fodor and D. L. V. Bauer, "The Structure of the Influenza A Virus Genome", *Nat. Microbiol.*, vol. 4, no. 11, pp. 1781-1789, 2019.

[14] M. Amin, O. Siddiqui, H. Abutarboush, M. Farhat and R. Ramzan, "A THz graphene metasurface for polarization selective virus sensing", *Carbon*, vol. 176, pp. 580-591, 2021.

[15] B. Wang, A. Sadeqi, R. Ma, P. Wang, W. Tsujita, K. Sadamoto, Y. Sawa, H. R. Nejad, S. Sonkusale, C. Wang et al, "Metamaterial Absorber for THz Polarimetric Sensing", In Proceedings of the SPIE, Terahertz, RF, Millimeter, and Submillimeter-Wave Technology and Applications XI, San Francisco, CA, USA, 2018, vol. 10531, pp. 1-7.

[16] F. Lan, F. Luo, P. Mazumder, Z. Yang, L. Meng, Z. Bao, J. Zhou, Y. Zhang, S. Liang, Z. Shi et al, "Dual-band refractometric terahertz biosensing with intense wave-matter-overlap microfluidic channel", *Biomed. Opt. Express*, vol. 10, pp. 3789-3799, 2019.